Thermochromic VO_2 Films with Periodic Meshes for Smart Windows: Analysis of Optical Properties

Chao Wang[a], Ling Li[a], Ye Tu[a], Jinming Zhang[a], Martina Schmid[b], Guanchao Yin[a*]

[a] School of Materials Science and Engineering, Wuhan University of Technology, Luoshi Road 122，430070 Wuhan, China

[b] Faculty of Physics & CENIDE, University of Duisburg-Essen, Lotharstraße 1, 47057 Duisburg, Germany

*Corresponding author: guanchao.yin@whut.edu.cn (Guanchao Yin)

ABSTRACT: VO_2 films with periodic meshes demonstrate the potential for application in smart windows. In this contribution, we theoretically study light propagating through meshed VO_2 films and identify three distinct optical phenomena, compared to their flat counterparts. The diffraction effect appears over the whole wavelength range from visible to infrared, contributing to an excellent luminous transmission (T_{lum}) beyond 60% and a relatively high solar transmission (T_{sol}) for broad geometry configurations. Local resonances arising from edge effect at the upper edge of the meshes and Wood's anomaly enable to drop T_{sol} in the infrared range for the condition above the critical temperature, which is desirable for improving the solar spectral modulation (ΔT_{sol}). However, they either tend to couple more part of resonance light into the meshes or are within a few discrete wavelengths only. Consequently, the transmission drop for VO_2 above the critical temperature is limited and thus results in a moderate ΔT_{sol}.

KEYWORDS: VO_2 films, Periodic meshes, Wood's anomaly, Edge effect, Solar spectral modulation

1 Introduction

Worldwide, around 30 to 40% of primary energy is consumed for residential buildings [1]. The background of global warming drives us to pursue innovative solutions for not only the mass production of clean energy but also the improvement of energy efficiency utilization. Smart windows, based on thermochromic materials coated on glass substrates, are very promising for improving the energy utilization of buildings because they can modulate the transmission of solar radiation upon temperature change, i.e. high infrared transmittance at low temperatures and low transmittance on hot days [2].

Among various thermochromic materials, vanadium dioxide (VO_2) stands out for its reversible metal-insulator transition (MIT) [3-5]. Below the critical temperature ($\tau_c = 68$ °C) VO_2 exhibits a monoclinic phase as an insulator allowing infrared transmission, while it switches to a metallic state and prevents infrared transmission above τ_c [3-5]. This unique feature allows to modulate indoor temperature, thus making VO_2 a promising candidate for smart windows [6-7]. However, from a practical

perspective, smart windows with coatings of thin VO_2 films show severe limitations in optical performance: Two key indicators are commonly defined for characterizing smart window performance, which are the transmission in the visible wavelength range (luminous transmission T_{lum}) and the difference in transmission at low and high temperatures (i.e. below and above the phase transition) for the entire solar spectral wavelengths (ΔT_{sol}) [3-7]. For regular VO_2 thin films these indicators take T_{lum}< 60% and ΔT_{sol}<15% only [8-12]. Due to the inherent absorption in luminous wavelengths, a thicker VO_2 film can improve ΔT_{sol} but at a cost of T_{lum} [13-14].

To address this issue, many attempts had been tested from the aspect of optical design, mainly comprising anti-reflection layer coating [14-18] and nano/micro structuring [19-24]. Among various optical strategies, a structure of VO_2 nano/micro meshes (thin films with periodic holes) was in the focus of investigation by several groups [21, 23-27] and a high T_{lum} beyond 80% was achieved [25]. Furthermore, the fabrication by nano/microsphere lithograph [28-29] is easily scalable at low cost. Last but not least, subwavelength metallic structures can excite localized surface plasmons [30-31], which offers potential to modify the transmission of VO_2. However, previous work was strongly related to experimental investigations and failed to explain the light propagation mechanisms of meshed VO_2, especially the moderate ΔT_{sol} (<10%). Inspired by these points, it will be of great importance to fully identify the optical mechanisms how the meshed structures interact with light and then explore the potential for an improved optical performance of meshed VO_2 structures.

In this contribution, we numerically study optical response of periodic meshes made from VO_2 films. Compared to the corresponding flat counterparts, there exist three extra distinct phenomena dominating optical responses of meshed VO_2 structures. The structure can be treated as a diffraction grating and the diffraction effect contributes to an excellent T_{lum} (beyond 60%) and T_{sol} for broad geometry configurations. Edge effect and Wood's anomaly are demonstrated to result in the drop of T_{sol}($>\tau_c$) and thus improve ΔT_{sol}. However, edge resonances tend to leak more part of the localized light energy into meshes and Wood's anomaly covers only a few discrete wavelengths. It contributes to a relatively limited drop of T_{sol} beyond τ_c and thus a moderate ΔT_{sol} (< 10%), which agrees well with experimental demonstrations [21, 23-27].

2 Simulations

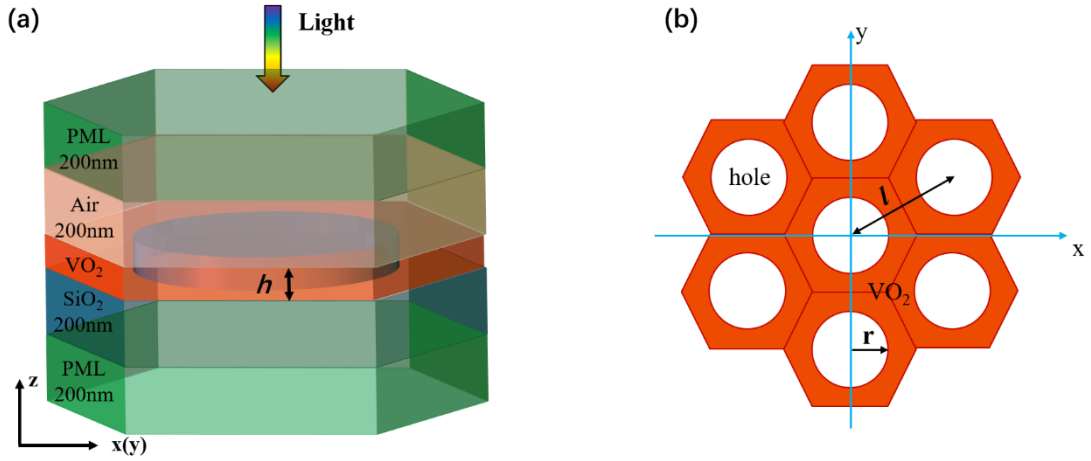

Figure 1 Sketch of (a) a unit cell of the simulation structure for meshed VO_2 films and (b) hexagonal periodicity of the meshes with a pitch *l* and a radius *r*

To study optical response of VO_2 films with periodic nano/micro meshes, we employ the finite element method (FEM) using the software COMSOL Multiphysics for 3D optical simulations. Figure 1(a) illustrates the unit cell of the simulation structure. It is composed of air/VO_2/glass from top to bottom with smooth interfaces. The mesh is made up from cylindrical holes penetrating the entire VO_2 layer and is treated as air. Three sets of periodic boundary conditions are applied in the x–y plane for a hexagonal computational domain. PML (perfectly matched layer) boundary conditions are set in the z direction. A plane wave source was introduced antiparallel to the z axis for assuming light incident from above the structure. Figure 1(b) shows the hexagonal periodicity of the mesh with a pitch *l* and a mesh radius *r*. Optical constants of VO_2 were taken from Ref. [18] and the refractive indices of air and glass were set to 1.0 and 1.5, respectively.

The luminous transmission T_{lum} and the solar transmission T_{sol} are defined according to the following equation [6-7]:

$$T_{lum/sol} = \frac{\int \varphi_{lum/sol}(\lambda) T(\lambda) d\lambda}{\int T(\lambda) d\lambda} \quad (1)$$

Where $\varphi_{lum/sol}(\lambda)$ is the solar spectrum under AM 1.5 solar irradiation condition over the respective wavelength range and $T(\lambda)$ the calculated transmittance. The subscript *sol* indicates the wavelength range of 350 -2500 nm and *lum* the luminous wavelength range of 350 - 780 nm. Besides, to quantify T_{lum} at both above and below τ_c, T_{lum} mentioned below is denoted as the averaged value:

$$T_{lum} = \frac{T_{lum}\ (<\tau_c) + T_{lum}\ (>\tau_c)}{2} \quad (2)$$

To evaluate the modulation ability of the solar spectrum for the meshed VO_2 films, the solar spectrum modulation is calculated as [6-7]:

$$\Delta T_{sol} = T_{sol}\ (<\tau_c) - T_{sol}\ (>\tau_c) \quad (3)$$

3 Results and Discussion

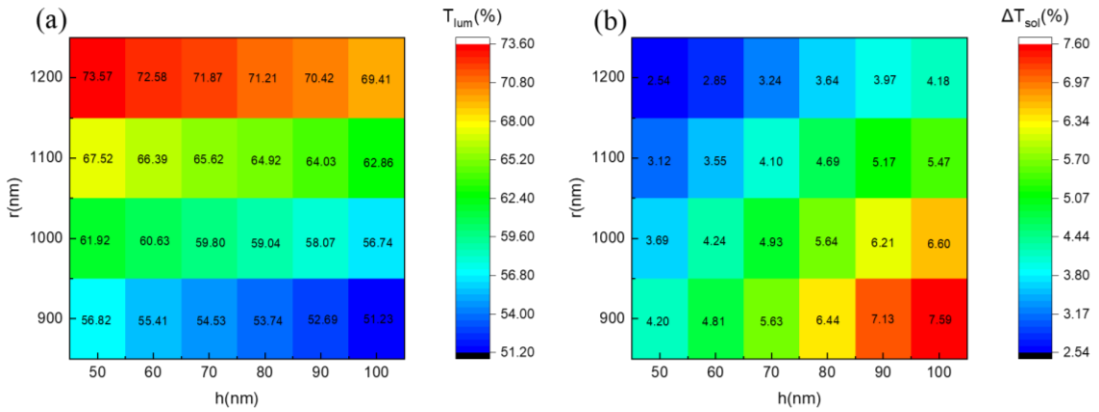

Figure 2 Contour plot of T_{lum} and ΔT_{sol} as a function of mesh height h and radius r

We start from a large pitch l of 2800 nm and plot in Figure 2 the contour image of T_{lum} and ΔT_{sol} as a function of height h of the VO_2 film and radius r of the hole (expressed as (h, r) in the following). The investigated r ranges from 900 to 1200 nm to avoid touching the holes whilst keeping a reasonable hole fraction for a superior T_{lum} and h is varied from 50 to 100 nm. On one hand, the meshed VO_2 structure can be treated as a 2-D diffraction grating. A larger radius corresponds to a higher diffraction efficiency and thereby benefits T_{lum}. On the other hand, a thicker VO_2 film and a smaller radius mean more volume interacting with incident light and thus produces more absorption in the metallic phase, which contributes to an improved ΔT_{sol}. It can be clearly observed that a smaller h combined with a larger r points to a greater T_{lum}, whereas ΔT_{sol} exhibits a reverse evolution trend. Consequently, the structure achieves the highest T_{lum} (73.7%) and the lowest ΔT_{sol} (2.54%) simultaneously at (h, r) = (50, 1200) nm, and the lowest T_{lum} (51.23%) and the optimum ΔT_{sol} (7.59%) at (h, r) = (100, 900) nm. Overall, a superior T_{lum} beyond 60% can be obtained with a quite moderate ΔT_{sol} below 10% for broad (h, r) configurations. A clarification is, to maintain a reasonable T_{lum}, both the combination of a larger mesh radius with a thicker film and the one of a smaller mesh radius with a thinner film are feasible. Considering that a thicker film is more favorable for a better ΔT_{sol} improvement, we select the configuration of a large mesh size combined with a relatively thick film for investigation here.

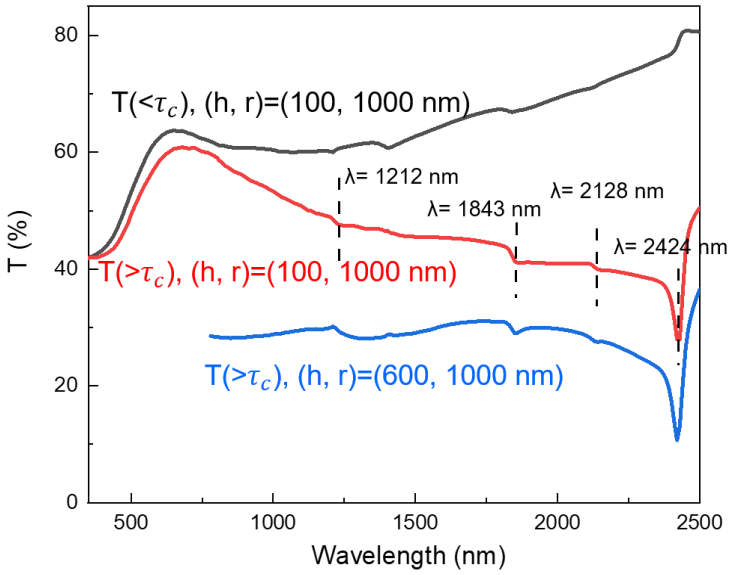

Figure 3 Transmission of the meshed VO_2 films

Figure 3 represents transmission curves for (h, r) = (100, 1000) nm. $T(<\tau_c)$ in the infrared wavelength range (780-2500 nm) is higher than 60% and even rises to 80% at 2500 nm. However, above τ_c, $T(>\tau_c)$ drops quite moderately with an average transmission value of 47% in the infrared wavelengths, which is responsible for the poor ΔT_{sol}. Therefore, in the following we will confine the investigation to light passing through the meshed VO_2 structure at temperature above τ_c.

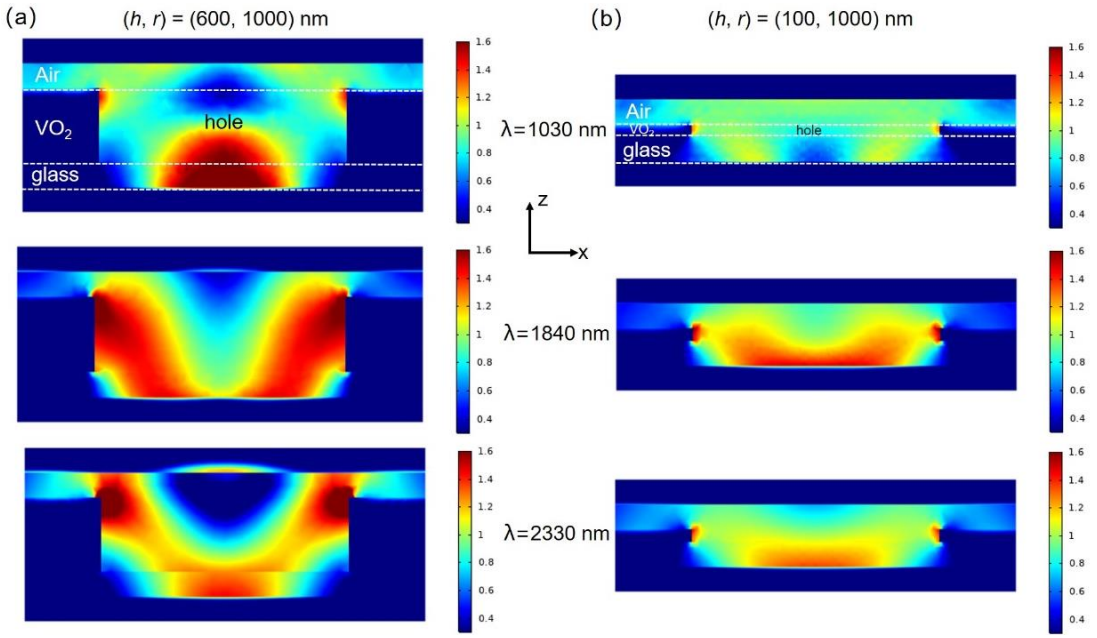

Figure 4 Near field intensity profiles of the meshed VO_2 structure for the configuration (a) (h, r) = (600, 1000) nm and (b) (h, r) = (100, 1000) nm at the wavelengths λ=1030, 1840, 2330 nm in x-z plane (the unit of the scale bar is $|E|^2/|E_0|^2$, where E_0 is the electric field of incident light).

It is widely proved that subwavelength metallic hole arrays can exhibit exceptional

transmission enhancement with pronounced and discrete transmission maxima, which is a net result of surface plasmon polaritons (SPPs) [32-33] and propagating modes [34]. However, both modes are not working here, which is beneficial for ΔT_{sol}. Firstly, discrete transmission enhancement peaks, which stem from SPPs, are not observed in Figure 3. The likely reason is that the bulk plasmon resonance is beyond the investigated wavelength range. Regarding propagating modes along the holes (z direction), these are not supported since the refractive index of the meshes (air) is less than that of the surrounding medium (VO_2). To identify how light transmits through the meshed structure, the configuration (h, r) = (600, 1000) nm is also simulated and the corresponding transmission curves are shown in comparison in Figure 3. h=600 nm can guarantee that light passing through the VO_2 matrix is completely absorbed in the infrared range and light can only propagate through the mesh array. $T(>\tau_c)$ for (h, r) = (600, 1000) nm is below 35% in the infrared wavelengths. Considering the mesh array occupying an area ratio of 46.25%, this implies that the propagating light through the mesh array indeed interacts with the VO_2 matrix and thus produces extra absorption. Figure 4(a) shows the representative near-field intensity profiles. Light is gradually focusing along the incident direction within the mesh. This is the typical feature of diffraction and contributes to $T(>\tau_c)$. Further, in the upper part of the inner wall of VO_2, the pronounced intensity confinement ($|E|^2/|E_0|^2 > 1$, E_0 is the electric field of incident light) is also observed. It is stressed here that this local confinement in the upper part of VO_2 meshes appears covering almost the whole investigated wavelengths. It is ascribed to the edge effect of light interacting with subwavelength features at the edge of the meshes, thus exciting localized resonances [35-36]. These resonances can partially produce extra absorption in the adjacent VO_2 matrix, which however tend to couple more light towards the mesh. Resultantly, the near-field intensity profiles visually explain that $T(>\tau_c)$ is lower than the transmission pointing to the zero-order diffraction (46.25%), yet the degree of transmission drop is limited. Figure 4(b) shows near-field intensity profiles for the configuration (h, r) = (100, 1000) nm as well and similar characteristics are observed. A thickness h = 100 nm of flat VO_2 films is not high enough to completely absorb the incident light. $T(>\tau_c)$ is therefore even higher for the meshed structure in the configuration of (h, r) = (100, 1000) nm compared to (h, r) = (600, 1000) nm. One point to be mentioned, is that the meshes have sharp edges in the simulation, which poses a challenge for experimental fabrications. We also simulated the condition for a certain amount of rounding on the edges and local resonances are still observed (Supporting information S1). Therefore, the results for the edge effect apply for experimental guidance.

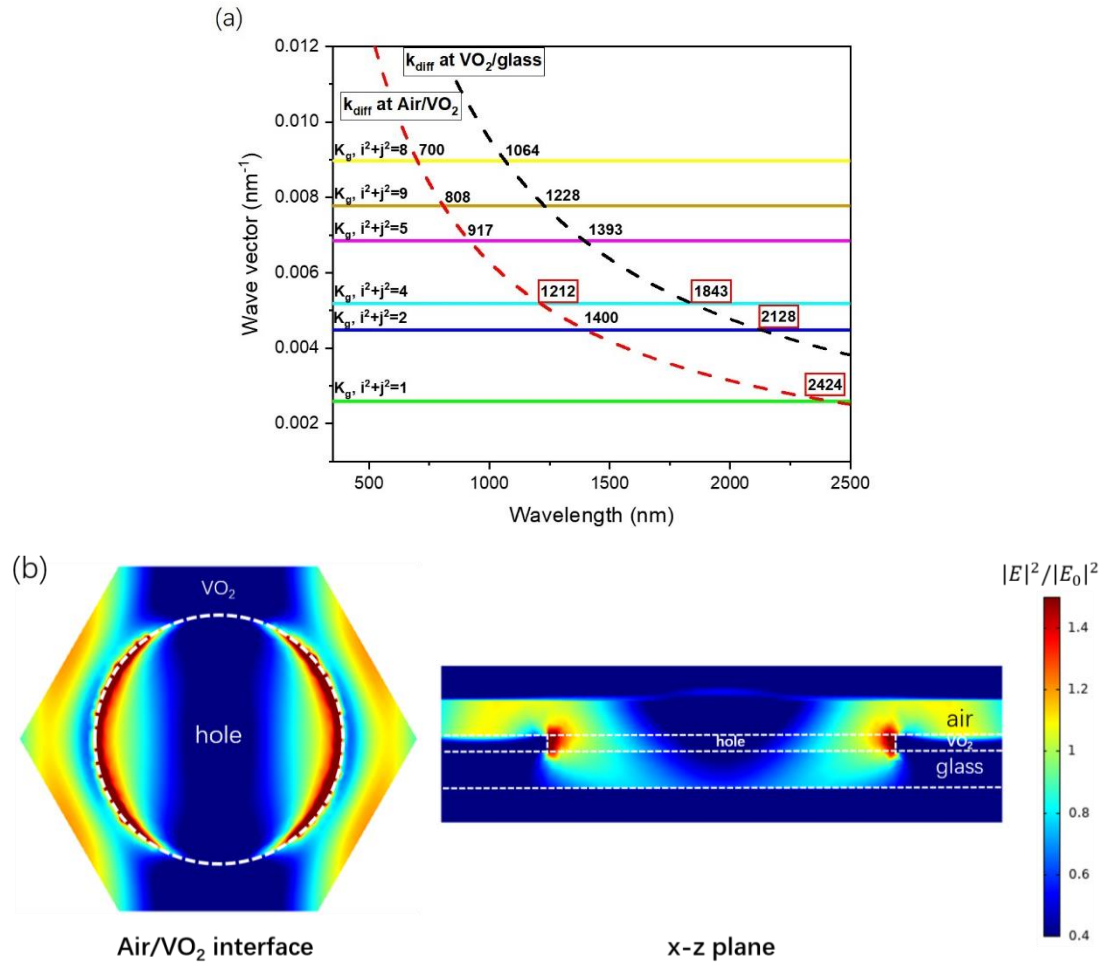

Figure 5 (a) k_{diff} and k_g as a function of wavelength at both air/VO_2 and VO_2/glass interfaces, (b) near field intensity profiles at the air/VO_2 interface and in the x-z plane at λ= 2424 nm

In Figure 3, there also exit four visible transmission minima in the $T(>\tau_c)$ curve at wavelengths λ = 1212, 1843, 2128 and 2424 nm, respectively. Further simulations varying the pitch reveal that the four transmission minima encounter a red-shift as pitch is increasing (see supporting information S2). This suggests that the minima are correlated to the pitch. We attribute this phenomenon to Wood's anomaly [33, 37], where the diffracted light in higher orders becomes tangent to the diffraction plane, resulting in an anomalous reduction in intensities. It fulfills the conservation of momentum that the wave vector of diffracted light (k_{diff}) equals to the grating momentum (k_g) in reciprocal space[33]:

$$k_{diff} = k_g \tag{4}$$

The wave vector is defined as $k_{diff} = 2\pi n/\lambda$, where n is the refractive index for incident or transmitted medium, and λ the wavelength of the incident light. It is $n = 1$ for air at the upper interface air/VO_2 and $n = 1.5$ for glass at the lower surface of VO_2/glass. The grating momentum is defined as $k_g = iG_x \pm jG_y$. G_x and G_y are the unit vectors in reciprocal space. They are in the periodic hexagonal lattice with an equal absolute value of $2\pi/l$ and an intersection angle of 60°, i, j are integers. Figure 5(a) plots

k_{diff} and k_g as a function of wavelength and we can identify thirteen discrete wavelengths where k_{diff} equals to k_g. The four characteristic wavelengths in Figure 3 are within them as the frames indicate. The Wood's anomaly exists at both the air/VO_2 and the VO_2/glass interface. Two peaks (λ=1212, 1843 nm) correspond to $i^2+j^2=4$, one (λ=2128 nm) to $i^2+j^2=2$ and one (λ=2424 nm) to $i^2+j^2=1$. Figure 5(b) exhibits the near field intensity profiles at λ=2424 nm. It can be clearly observed that light is strongly coupled along the surface of VO_2 and propagates into the VO_2 matrix. Due to the absorption ability of VO_2, this brings absorption enhancement and thus reduces $T(>\tau_c)$.

It is noted that, among the four transmission minima arising from Wood's anomaly, the transmission reduction at the longest wavelength λ=2424 nm (corresponding to $i^2+j^2=1$) is the most pronounced, which is a joint effect of two points. Firstly, VO_2 exhibits a higher absorption ability (a higher extinction coefficient) at longer wavelengths in the infrared range. Further, the wavelength corresponding to $i^2+j^2=1$ points to the highest coupling efficiency of light along the air/VO_2 interface. As the near field profiles in Figure 5(b) show, the maximum $|E|^2/|E_0|^2$ at the coupling interface is above 1, which is not reached for the other three characteristic wavelengths (not shown here). Further increasing the pitch l, the characteristic wavelength corresponding to $i^2+j^2=1$ will red-shift beyond 2500 nm, which is out of the wavelength range of interest. Therefore, setting the pitch l= 2800 nm in this work has two advantages. It enables the longest characteristic wavelength close to the wavelength limit of 2500 nm and therefore supports the most pronounced transmission reduction. Moreover, according to Equation 4, a larger pitch can support more discrete transmission minima especially in the infrared range, which is desirable for ΔT_{sol} improvement.

4 Conclusion

In this work, we investigated the optical responses of thermochromic VO_2 films with periodic meshes. Due to the strong inherent diffraction effect, the meshed VO_2 structures exhibit an excellent T_{lum} (beyond 60%) at broad geometry configurations. Simultaneously, it also brings a relatively high $T(>\tau_c)$, which is mainly responsible for the moderate ΔT_{sol}. The local edge effect excited at the upper edge of the meshes indeed produces extra absorption in broadband wavelengths, which however tends to couple more light into the hole rather than the VO_2 matrix. Wood's anomaly can significantly drop transmission as well but is limited to a few discrete wavelengths. Resultantly, the meshed VO_2 structures can bring a moderate effect with respect to the transmission drop in the infrared range and therefore contribute to a moderate ΔT_{sol} below 10%. Overall, the study well explains that why the meshed VO_2 structure can achieve a superior T_{lum} but a moderate ΔT_{sol} in experimental demonstrations [21, 23-27].

ACKNOWLEDGEMENTS

C. Wang, N. Ling, Y. Tu, J. M. Zhang and G. Yin would like to thank the funding from National Natural Science Foundation of China (NSFC: 51802240) and the funding

support of the Fundamental Research Funds for the Central Universities (WUT:183101002, 193201003).

Reference

[1] T. Ramesh, R. Prakash, K. K. Shukla, Life cycle energy analysis of buildings: An overview. Energy Build. 42, 1592–1600 (2010).

[2] R. Baetens, B. P. Jelle, A. Gustavsen, Properties, requirements and possibilities of smart windows for dynamic daylight and solar energy control in buildings: A state-of-the-art review. Sol. Energy Mater. Sol. Cells 94, 87–105 (2010).

[3] R. M. Wentzcovitch, W. W. Schulz, P. B. Allen, VO2: Peierls or Mott-Hubbard? A view from band theory. Phys. Rev. Lett. 72, 3389–3392 (1994).

[4] M. M. Qazilbash, M. Brehm, B.-G. Chae, P.-C. Ho, G. O. Andreev, B.-J. Kim, S. J. Yun, A. V. Balatsky, M. B. Maple, F. Keilmann, H.-T. Kim, D. N. Basov, Mott transition in VO2 revealed by infrared spectroscopy and nano-imaging. Science 318, 1750–1753 (2007).

[5] N. B. Aetukuri, A. X. Gray, M. Drouard, M. Cossale, L. Gao, A. H. Reid, R. Kukreja, H. Ohldag, C. A. Jenkins, E. Arenholz, K. P. Roche, H. A. Dürr, M. G. Samant, S. S. P. Parkin, Control of the metal-insulator transition in vanadium dioxide by modifying orbital occupancy. Nat. Phys. 9, 661–666 (2013).

[6] Y. Cui, Y. Ke, C. Liu, Z. Chen, N. Wang, L. Zhang, Y. Zhou, S. Wang, Y. Gao, Y. Long, Thermochromic VO2 for Energy-Efficient Smart Windows. Joule 2, 1707–1746 (2018)

[7] X. Cao, T. Chang, Z. Shao，F. Xu, H. Luo, P. Jin, Challenges and Opportunities toward Real Application of VO2-Based Smart Glazing. Matter 2, 862–881 (2020)

[8] S.-Y. Li, G. A. Niklasson, C. G. Granqvist, Thermochromic fenestration with VO2-based materials: Three challenges and how they can be met. Thin Solid Films 520, 3823–3828 (2012).

[9] M. Li, S. Magdassi, Y. Gao, Y. Long, Hydrothermal synthesis of VO2 polymorphs: Advantages, challenges and prospects for the application of energy efficient smart windows. Small 13, 1701147 (2017).

[10] S. Wang, M. Liu, L. Kong, Y. Long, X. Jiang, A. Yu, Recent progress in VO2 smart coatings: Strategies to improve the thermochromic properties. Prog. Mater. Sci. 81, 1–54 (2016).

[11] Q. Liu, C. Liu, N. Wang, S. Magdassi, D. Mandler, Y. Long, Periodic micro-patterned VO2 thermochromic films by mesh printing. J. Mater. Chem. C 4, 8385-8391(2016).

[12] L. Kang, Y. Gao, H. Luo, Z. Chen, J. Du, Z. Zhang, Nanoporous Thermochromic VO2 Films with Low Optical Constants, Enhanced Luminous Transmittance and Thermochromic Properties. ACS Appl. Mater. Interfaces, 3,135-138 (2011).

[13] Z. Zhang, Y. Gao, Z. Chen, J. Du, C. Cao, L. Kang, H. Luo, Thermochromic VO2 Thin Films: Solution-Based Processing, Improved Optical Properties, and Lowered Phase Transformation Temperature. Langmuir 26, 10738-10744 (2010).

[14] G. Xu, P. Jin, M. Tazawa, K. Yoshimura, Optimization of antireflection coating for VO2-based energy efficient window. Sol. Energy Mater. & Sol. Cells 83, 29–37 (2004).

[15] N. R. Mlyuka, G. A. Niklasson, C. G. Granqvist, Thermochromic VO2-based multilayer films with enhanced luminous transmittance and solar modulation. Phys. Status Solidi A 206, 2155–2160 (2009).

[16] P. Jin, G. Xu, M. Tazawa, K. Yoshimura, Design, formation and characterization of a novel multifunctional window with VO2 and TiO2 coatings. Appl. Phys. A 77, 455–459 (2003).

[17] H. Liu, H. Song, H. Xie, G. Yin, Enhanced optical performance of thermochromic VO2 based on multilayer designs. Eur. Phys. J. Appl. Phys. 88, 30301 (2019)

[18] N. R. Mlyuka, G. A. Niklasson, C. G. Granqvist, Thermochromic multilayerfilmsof VO2 and TiO2 with

enhanced Transmittance. Sol. Energy Mater. Sol. Cells 93,1685–1687 (2009).
[19] D. Li, M. Li, J. Pan, H. Wu, Y. Zhang, G. Li, Hydrothermal synthesis of Mo-doped VO2/TiO2 composite nanocrystals with enhanced thermochromic performance. ACS Appl. Mater. Interfaces 6, 6555–6561(2014).
[20] Q. Lu, C. Liu, N. Wang, S. Magdassi, D. Mandler, Y. Long. Periodic micro-patterned VO2 thermochromic films by mesh printing. J. Mater. Chem. C 4, 8385–8391 (2016).
[21] Y.J. Ke, X.L. Wen, D.Y. Zhao, R.C. Che, Q.H. Xiong, Y. Long. Controllable fabrication of two-dimensional patterned VO2 nanoparticle, nanodome, and nanonet arrays with tunable temperature-dependent localized surface plasmon resonance. ACS Nano 11, 7542–7551 (2017).
[22] A. Taylor, I. Parkin, N. Noor, C. Tummeltshammer, M. S. Brown, I. Papakonstantinou. A bioinspired solution for spectrally selective thermochromic VO2 coated intelligent glazing. Opt. Exp. 21, A750 (2013).
[23] M. Liu, B. Su, Y. Kaneti, Z. Chen, Y. Tang, Y. Yuan, Y. Gao, L. Jiang, X. Jiang, A. Yu. Dual-Phase Transformation: Spontaneous Self-Template Surface-Patterning Strategy for Ultra-transparent VO2 Solar Modulating Coatings. ACS Nano 11, 407-415 (2017).
[24] C. Liu, I. Balin, S. Magdassi, I. Abdulhalim, Y. Long. Vanadium dioxide nanogrid films for high transparency smart architectural window applications. Opt. Exp. 23, A124 (2015).
[25] M. Zhou, J. Bao, M. Tao, R. Zhu, Y. Lin, X. Zhang, Y. Xie. Periodic porous thermochromic VO2(M) films with enhanced visible transmittance. Chem. Commun. 49, 6021-6023 (2013)
[26] H. Li, H. Djaoued, J. Robichaud, Y. Djaoued. A pleasant blue-green colored 2D vanadium dioxide inverse opal monolayer: large area fabrication and its thermochromic application. J. Mater. Chem. C 8, 11572-11580 (2020)
[27] R. Sun, B. Jin, L. Yao, Y. Liu, J. Li, J. Liang, J. He. Controllable Design of Bifunctional VO2 Coatings with Superhydrophobic and Thermochromic Performances. ACS Appl. Mater. Interfaces. 13, 13751–13759 (2021)
[28] X. Ye, L. Qi. Two-Dimensionally Patterned Nanostructures Based on Monolayer Colloidal Crystals: Controllable Fabrication, Assembly, and Applications. Nano Today 6, 608−631 (2011).
[29] M. Fang, H. Lin, H. Y. Cheung, F. Xiu, L. Shen, S. Yip, E. Y. B. Pun, C. Y. Wong, J. C. Ho. Polymer-Confined Colloidal Monolayer: A Reusable Soft Photomask for Rapid Wafer-Scale Nanopatterning. ACS Appl. Mater. Interfaces 6, 20837−20841 (2014).
[30] K. R. Catchpole, A. Polman. Plasmonic solar cells. Opt. Express, 16, 21793−21800 (2008).
[31] H. Atwater, A. Polman. Plasmonics for Improved Photovoltaic Devices. Nat. Mater. 9, 205−213 (2010).
[32] T. W. Ebbesen, H. J. Lezec，T. Thio，P. A. Woff. Extraordinary optical transmission through sub-wavelength hole arrays. Nature 391, 667-669 (1998).
[33] H. F. Ghaemi, T. Thio. D. E. Grupp, T. W. Ebbesen, H. J. Lezec. Surface plasmons enhance optical transmission through subwavelength holes. Phys. Review B 58. 6779-6782 (1998).
[34] H. Shin, P. B. Catrysse, S. Fan. Effect of the plasmonic dispersion relation on the transmission properties of subwavelength
cylindrical holes. Phys. Review B 72. 085436 (2005).
[35] X. Y. Gu, P. F. Gao, H. Y. Zou, J. H. Liu, Y. F. Li, C. Z. Huang. The localized surface plasmon resonance induced edge effect of gold regular hexagonal nanoplates for reaction progress monitoring. Chem. Commun. 54, 13359-13362 (2018).
[36] J. C. Hsu, C. H. Hsu. Edge waves and resonances in two-dimensional phononic crystal plates. J. Appl. Phys. 117, 174504 (2015).
[37] R. W. Wood. Anomalous Diffraction Gratings. Phys. Rev. 48, 928-936 (1935).

Supporting information

S1:

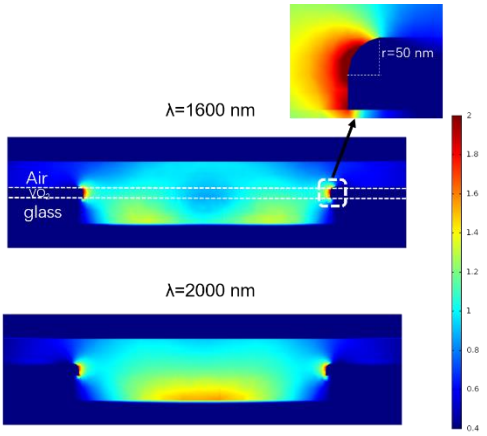

Figure S1 Representative near field intensity profiles of the meshed VO_2 structure for the configuration (h, r) = (100, 1000) nm and a rounding at the upper edge of meshes at the wavelengths λ=1600, 2000 nm in x-z plane (the unit of the scale bar is |E|^2/|E_0 |^2, where E0 is the electric field of incident light). The rounding is realized assuming a quarter of circle with a radius of 50 nm

S2: pitch change

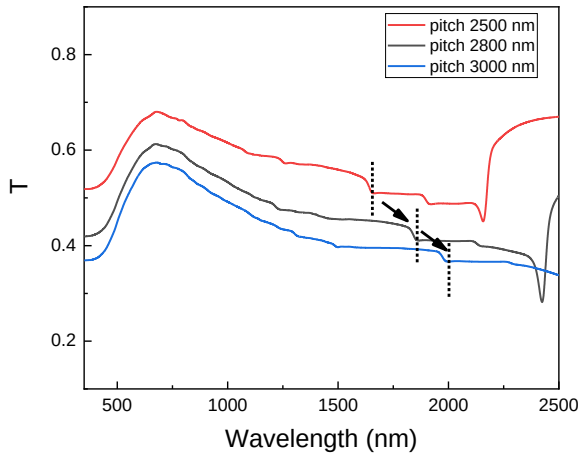

Figure S2 Shift of characteristic wavelengths arising from Wood's anomaly depending on the pitch for (h, r) = (100, 1000) nm.